

Electronic and thermal properties of Ag-doped single crystal zinc oxide via laser-induced technique

Huan Xing(邢欢), Hui-Qiong Wang(王惠琼), Tinglu Song(宋廷鲁), Chunli Li(李纯莉), Yang Dai(戴扬), Gengming Fu(傅耿明), Junyong Kang(康俊勇), and Jin-Cheng Zheng(郑金成)
Citation: Chin. Phys. B, 2023, 32 (**6**): 066107. DOI: 10.1088/1674-1056/acae74
Journal homepage: http://cpb.iphy.ac.cn; http://iopscience.iop.org/cpb

What follows is a list of articles you may be interested in

Migration of weakly bonded oxygen atoms in a-IGZO thin films and the positive shift of threshold voltage in TFTs

Chen Wang(王琛), Wenmo Lu(路文墨), Fengnan Li(李奉南), Qiaomei Luo(罗巧梅), and Fei Ma(马飞)†
Chin. Phys. B, 2022, 31 (**9**): 096101. DOI: 10.1088/1674-1056/ac560f

Oxygen vacancies and V co-doped Co_3O_4 prepared by ion implantation boosts oxygen evolution catalysis

Bo Sun(孙博), Dong He(贺栋), Hongbo Wang(王宏博), Jiangchao Liu(刘江超), Zunjian Ke(柯尊健), Li Cheng(程莉), and Xiangheng Xiao(肖湘衡)
Chin. Phys. B, 2021, 30 (**10**): 106102. DOI: 10.1088/1674-1056/ac1339

Improved carrier transport in Mn:ZnSe quantum dots sensitized La-doped nano-TiO_2 thin film

Shao Li(李绍), Gang Li(李刚), Li-Shuang Yang(杨丽爽), Kui-Ying Li(李葵英)
Chin. Phys. B, 2020, 29 (**4**): 046104. DOI: 10.1088/1674-1056/ab7742

Synthesis of Pr-doped ZnO nanoparticles: Their structural, optical, and photocatalytic properties

Jun-Lian Chen(陈军联), Neena Devi, Na Li(李娜), De-Jun Fu(付德君), Xian-Wen Ke(柯贤文)
Chin. Phys. B, 2018, 27 (**8**): 086102. DOI: 10.1088/1674-1056/27/8/086102

Synthesis and magnetotransport properties of Bi_2Se_3 nanowires

Kang Zhang(张亢), Haiyang Pan(潘海洋), Zhongxia Wei(魏仲夏), Minhao Zhang(张敏昊), Fengqi Song(宋凤麒), Xuefeng Wang(王学锋), Rong Zhang(张荣)
Chin. Phys. B, 2017, 26 (**9**): 096101. DOI: 10.1088/1674-1056/26/9/096101

SPECIAL TOPIC — Celebrating the 100th Anniversary of Physics Discipline of Xiamen University

Electronic and thermal properties of Ag-doped single crystal zinc oxide via laser-induced technique

Huan Xing(邢欢)[1], Hui-Qiong Wang(王惠琼)[1,2,†], Tinglu Song(宋廷鲁)[3,‡], Chunli Li(李纯莉)[4], Yang Dai(戴扬)[5], Gengming Fu(傅耿明)[1], Junyong Kang(康俊勇)[1], and Jin-Cheng Zheng(郑金成)[1,2,§]

[1] *Engineering Research Center of Micro-nano Optoelectronic Materials and Devices, Ministry of Education; Fujian Key Laboratory of Semiconductor Materials and Applications, CI Center for OSED, and Department of Physics, Xiamen University, Xiamen* 361005, *China*

[2] *Department of Physics and Department of New Energy Science and Engineering, Xiamen University Malaysia, Sepang* 439000, *Malaysia*

[3] *Experimental Center of Advanced Materials, School of Materials Science & Engineering, Beijing Institute of Technology, Beijing* 100081, *China*

[4] *School of Material Science & Engineering, Beijing Key Laboratory of Environmental Science and Engineering, Beijing Institute of Technology, Beijing* 100081, *China*

[5] *Department of Chemical Engineering, School of Environmental and Chemical Engineering, and Institute for Sustainable Energy, Shanghai University, Shanghai* 200444, *China*

(Received 23 November 2022; revised manuscript received 22 December 2022; accepted manuscript online 27 December 2022)

The doping of ZnO has attracted lots of attention because it is an important way to tune the properties of ZnO. Post-doping after growth is one of the efficient strategies. Here, we report a unique approach to successfully dope the single crystalline ZnO with Ag by the laser-induced method, which can effectively further post-treat grown samples. Magnetron sputtering was used to coat the Ag film with a thickness of about 50 nm on the single crystalline ZnO. Neodymium-doped yttrium aluminum garnet (Nd:YAG) laser was chosen to irradiate the Ag-capped ZnO samples, followed by annealing at 700 °C for two hours to form ZnO:Ag. The three-dimensional (3D) information of the elemental distribution of Ag in ZnO was obtained through time-of-flight secondary ion mass spectrometry (TOF-SIMS). TOF-SIMS and core-level x-ray photoelectron spectroscopy (XPS) demonstrated that the Ag impurities could be effectively doped into single crystalline ZnO samples as deep as several hundred nanometers. Obvious broadening of core level XPS profiles of Ag from the surface to depths of hundred nms was observed, indicating the variance of chemical state changes in laser-induced Ag-doped ZnO. Interesting features of electronic mixing states were detected in the valence band XPS of ZnO:Ag, suggesting the strong coupling or interaction of Ag and ZnO in the sample rather than their simple mixture. The Ag-doped ZnO also showed a narrower bandgap and a decrease in thermal diffusion coefficient compared to the pure ZnO, which would be beneficial to thermoelectric performance.

Keywords: zinc oxide, Ag-doping, laser-induced technique, XPS, SIMS, thermal diffusivity

PACS: 61.72.uj, 81.05.Dz, 65.40.–b **DOI:** 10.1088/1674-1056/acae74

1. Introduction

ZnO is an important optoelectronic semiconductor because of its unique properties such as direct wide band gap of 3.37 eV, and large exciton binding energy (60 meV).[1] Several strategies have been applied to tune the properties of ZnO. Interesting properties and application of ZnO through nanostructuring have been reported,[2] including two-dimensional nanosheets,[3] one-dimensional nanoribbons,[4] nanowires,[5] and nanotubes,[6] as well as zero-dimensional nanoclusters,[7] nanocages,[8] and nanorings,[9] *etc.* Interfacing of ZnO with other oxides is also important to extend the applications of ZnO-based devices.[10–12]

Both theoretical and experimental studies have shown that doping can effectively elevate the physical and chemical properties of ZnO.[13] Over the last few years it has been suggested to use group IB element as dopant to regulate its photoelectric properties.[14–17] Silver is an extraordinarily general group IB element, and it can provide an acceptor energy level when it becomes a substitution impurity by replacing Zn.[18] Growth and characterization of Ag-doped zinc oxides have been reported. Low-resistance p-type zinc oxides doped via silver were obtained with the pulsed laser deposition (PLD) method.[19] Ag–N co-doping thin films were realized by Swapna *et al.* using the spray pyrolysis technique, and the thin film exhibited high hole concentration (2.1×10^{18} cm^{-3}) and low resistivity (8.70×10^{-2} Ω·cm).[20]

Alternatively, post-doping processes can be utilized after the thin film growth, which provides more flexibility of doping elements and the localization of doping areas. The laser-induced method is one of the post-doping processes. Laser-induced techniques have been broadly used in a number of fields, especially in the area of material fabrication process-

†Corresponding author. E-mail: hqwang@xmu.edu.cn
‡Corresponding author. E-mail: song@bit.edu.cn
§Corresponding author. E-mail: jczheng@xmu.edu.cn

© 2023 Chinese Physical Society and IOP Publishing Ltd

ing. The capped material is melted by using the laser processing technology. During the process, the impurity elements can be diffused into the lattice of the substrate for the doping purpose. Compared with the traditional doping, the laser-induced technique has obvious advantages. Local diffusion can be controlled through the adjustment of the heating temperature. Furthermore, compared with some conventional diffusion processes such as ion implantation, which requires photolithography, etching, and other processes, laser-induced diffusion is just a one-step process. Chen *et al.*[21] used Nd:YAG lasers for laser irradiation to reap supersaturated Ni doping on the p-type silicon wafer substrate; Aoki *et al.*[22] efficiently fabricated the homogeneous zinc oxide p–n junctions using the KrF laser induction, which showed ultraviolet luminescence; Choi *et al.*[23] produced the p-doped single-layer graphene using the XeCl laser; Tian *et al.*[24] used the Nd:YAG laser and excimer laser to realized N doping and Al doping in SiC, respectively. It is also worth pointing out that the laser-induced methods have a wide range of applications in magnetic materials. Chizhik *et al.*[25] prepared Co-doped yttrium iron garnet films and irradiated the films with an argon laser beam. They demonstrated the existence of the polarization-sensitive photomagnetic effect light-induced magnetization process in the films at room temperature.

Besides ionic doping, nano-inclusion of element has also raised research attention, in particular to enhance thermoelectric performance.[26–29] The fabricated samples will also be suitable candidates to investigate the possible influence of thermal-related properties due to the asymmetry of elemental distribution.[30] In this study, Ag-doped ZnO was synthesized using a continuous-wave (CW) laser to continuously irradiate ZnO crystals covered with Ag films. The lattice structure and electronic state as well as the doping concentration of Ag at different depths were investigated, which demonstrated the effective doping utilizing the laser-induced method.

2. Experimental details

The fabrication process of the ZnO:Ag (laser-induced Ag-doped ZnO) is shown in Fig. 1(a). Firstly, the magnetron sputtering system was utilized to deposit a 50-nm thick silver film uniformly on a monocrystalline ZnO (002) substrate (size = 5 mm × 10 mm, thickness = 0.5 mm). After that, the Ag/ZnO (ZnO sample with the deposited silvercapped thin film) was placed in the CW laser chamber. In order to prevent sample damage due to excessive laser energy during scanning, the substrate temperature was maintained at 723 K, and Ar was filled in the cavity as an inert protective gas, while the pressure was kept inside the cavity at 1 atm (1 atm = 1.01325×10^5 Pa). The sample was scanned twenty times by the laser at a uniform speed of 2 mm/s. During the laser irradiation process, the silver atoms were diffused into the zinc oxide lattice after the absorption of thermal energy. Finally, the treated samples were washed to remove surface organics, dried, and annealed at 973 K for two hours.

Figure 1(b) illustrates the schematic of scanning process using a special CW laser (Nd:YAG) apparatus. The CW laser apparatus consists of a linear-type CW laser, a quartz sample holder and a temperature-controlled heating unit. The energy density of the linear laser beam focused on the sample surface was quasi-homogenous in the directions of length and width, and the size of the laser was 1 mm × 1 cm.

The laser wavelength used in this paper was 1.06 μm, and the laser power was 250 W. The hydrothermally grown zinc oxide single crystals were purchased from HF-Kejing Co. Ltd. The elemental depth distribution information of the Ag-doped sample was investigated by the time of flight-secondary ion mass spectrometer (TOF-SIMS, PHI nano TOF II, ULVAC-PHI Inc. Japan). Lattice information was probed by x-ray diffractometer (XRD-7000, Shimadzu Analytical India Ltd. Japan). Electronic state was investigated by x-ray photoelectron spectroscopy (XPS, Thermo Scientific ESCALAB Xi^+, Thermo Fisher, USA). Measurements of thermal diffusivity were conducted using laser flash apparatus (LFA 457, Netzsch Ltd., Germany).

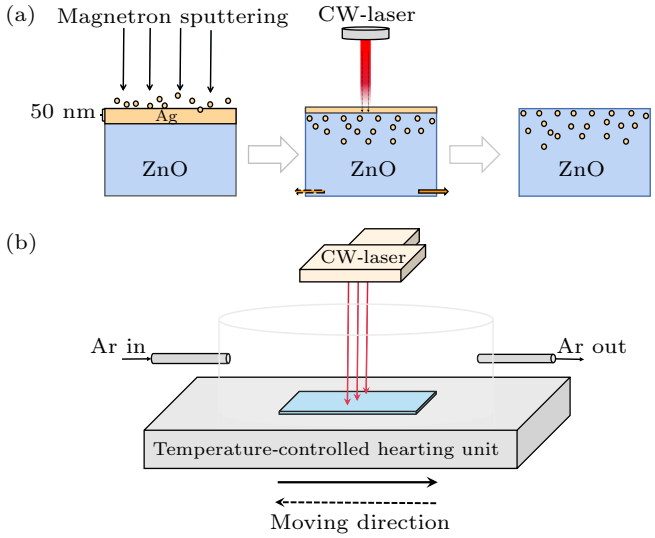


Fig. 1. Laser-induced doping method: (a) the fabrication process of the ZnO:Ag, (b) schematic diagram of scanning process using the CW laser apparatus.

3. Results and discussion

3.1. Depth profile

Figure 2 shows the x-ray diffraction (XRD) of comparison of ZnO and ZnO:Ag, where the red line indicates the sample of the untreated ZnO substrate, and the black line indicates the Ag-doped ZnO sample after the laser-induced treatment. The most prominent signal of ZnO (002) shows that the laser-induced sample still maintains the crystal structure of ZnO and the crystal orientation of *c* axis. It can also be seen that there

is an obvious peak at around 38.1°, which could be associated with Ag (111) [38.1°] and/or Ag_2O (200) [38.07°]. Meanwhile, the peak positions of untreated and laser-induced ZnO (002) are at 34.51° and 34.39°, respectively. The shift is corresponding to an increase of lattice parameter along the *c* axis, which could be resulted from the replacement of Zn^+ with an iron radius of 0.72 Å by Ag^+ with a larger ion radius of 1.22 Å.[19]

Figure 3 exhibits the scanning electron microscope (SEM) image of the surface (a) and the cross-section (b) of the ZnO:Ag sample. It can be seen that the surface of the sample irradiated by laser absorbs the energy of the laser to melt and then recrystallizes, and the surface after recrystallization is smooth. Besides, white spherical silver nanoparticles can be seen, which is attributed to the fact that some of the melted silver failed to diffuse into the ZnO substrate successfully, however, solidified on the surface to structure silver nanoparticles, which are not obviously visible in the cross-section. As showed in the cross-section SEM image (Fig. 3(b)), the single-crystal structure of the sample after laser induction can be determined, which is consistent with the XRD results. Table 1 shows the atomic ratios of the Zn/Ag from the energy dispersive spectroscopy (EDS) results of the ZnO:Ag sample, which indicates the decrease of the Ag concentration from the surface to the cross-section of the sample, in agreement with the SEM images.

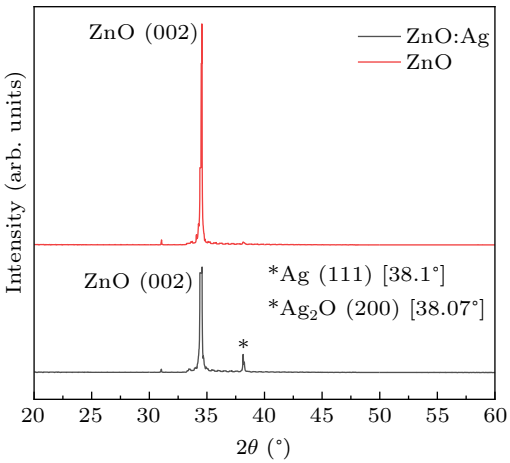


Fig. 2. X-ray diffraction patterns of ZnO and ZnO:Ag.

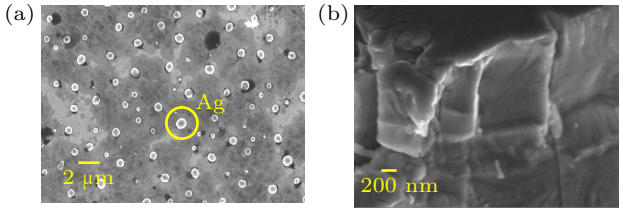


Fig. 3. Scanning electron microscope (SEM) images of the surface (a) and cross-section (b) of the ZnO:Ag sample.

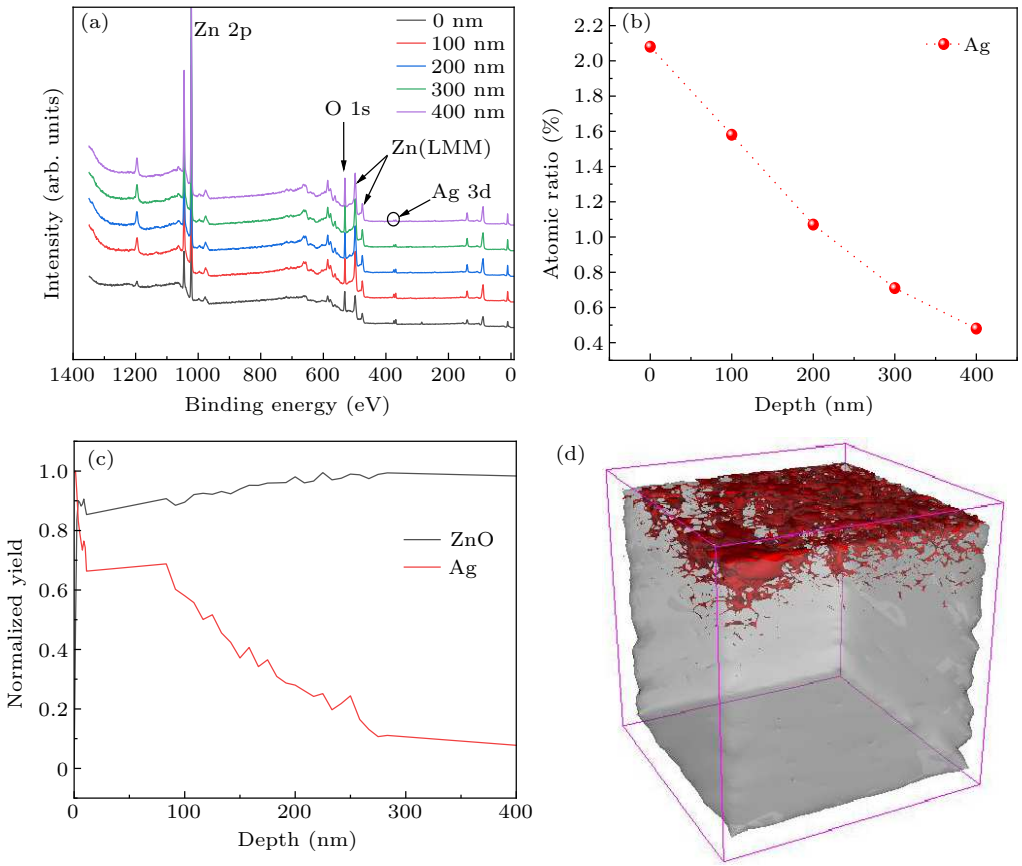


Fig. 4. Element analyses of ZnO:Ag: (a) XPS spectra depth profile of the ZnO:Ag sample, (b) the atomic proportion of Ag calculated by Ag 3d XPS with the high resolution mode, (c) TOF-SIMS depth profile of the ZnO:Ag sample, (d) 3D distribution of Ag in the ZnO lattice by TOF-SIMS.

Table 1. The Atomic ratio of Zn and Ag measured by EDS.

Sample area	Ratio of Zn:Ag atomic concentration
Surface	1:0.048
Cross-section	1:0.027

Table 2. The atomic ratio of Zn and Ag measured by XPS.

Depth (nm)	Ratio of the Zn:Ag (atomic concentration)
0	1:0.040
100	1:0.027
200	1:0.018
300	1:0.017
400	1:0.008

Figure 4(a) is an XPS survey as a function of depth. Figure 4(b) shows the decreasing trend of the Ag concentration with the increase of depth, in agreement with the ratio of Zn/Ag atomic concentration as a function of thickness determined by XPS as illustrated in Table 2. Additionally, the relative concentration changes of Ag and ZnO with depth are given through the TOF-SIMS depth profile, as shown in Fig. 4(c). It can be observed that the concentration of ZnO slightly increases from the surface area and maintains almost constant beneath the surface, while the concentration of Ag decreases gradually with the increase of the depth. Figure 4(d) presents the 3D distribution of Ag element distribution, from which the distribution of Ag (red portion) element in the ZnO (grey portion) lattice can be virtually seen. The SIMS results are in good agreement with XPS and SEM/EDS results.

3.2. Electronic state evolution

The detailed electronic state evolution analysis of ZnO:Ag is given by core level XPS of Zn 2p, O 1s, and Ag 3d peaks in the narrow-scan mode. Figure 5(a) shows the core level XPS of Zn 2p with obvious doublet features of Zn $2p^{1/2}$ and Zn $2p^{3/2}$ due to spin–orbit splitting. The depth profiles of the peak positions (in solid line with symbol) and full width at half maximum (FWHM, in dotted line with symbol) of the Zn $2p^{1/2}$ and Zn $2p^{3/2}$ peaks are illustrated in Fig. 5(b). It can be seen that the peak positions of the Zn $2p^{1/2}$ and Zn $2p^{3/2}$ peaks remain at 1044.8 eV and 1021.8 eV, respectively, with a distance of 23 eV.[31] Interestingly, the FWHM values of the Zn $2p^{1/2}$ peak and Zn $2p^{3/2}$ peak were 2.27 eV and 1.89 eV, respectively, on the surface, which were reduced to 1.81 eV and 1.66 eV, respectively, for the depth between 100 nm and 400 nm. This could be due to the high concentrations of doped Ag on the surface, which led to the change of chemical environment for the Zn ions.

Figure 5(c) displays the core level XPS spectra of Ag 3d, showing the spin–orbit splitting features of Ag $3d^{5/2}$ and Ag $3d^{3/2}$ peaks. The depth profiles of the Ag 3d XPS peak positions (in solid lines) and the FWHM values (in dotted lines) are exhibited in Fig. 5(d). The peak positions of Ag $3d^{3/2}$ and Ag $3d^{5/2}$ spectra show slight fluctuations at different depths, however, their distances maintain 6 eV.[32–34] Meanwhile, the FWHM of Ag $3d^{3/2}$ and Ag $3d^{5/2}$ has been detected. Their values on the surface are smaller due to the higher concentration of silver on the surface, which causes the chemical state of Ag on the surface to be less affected by zinc oxide.

Figure 5(e) shows the core level XPS of O 1s for different depths, which is decomposed into two Gaussians peaks, one main peak of the O 1s of ZnO (530.2 eV) and one satellite peak (532.4 eV) that could be originated from the Ag doping that alter the oxide environment (thus labelled as Ag–Zn–O O 1s).[35] The O 1s peaks around the surface area were not included to exclude the influence of surface contamination. Figure 5(f) shows the comparison of the evolution of the peak positions and the FWHM values for the two peaks as a function of film thickness. It can be seen that the binding energy positions of the two peaks are essentially unshifted, as well as the FWHM value of ZnO O 1s. Only some fluctuations are observed for the FWHM value of the Zn–Ag–O O 1s. The result agrees with that in Fig. 5(b).

Figure 6(a) is the valence band XPS of ZnO, which usually consists of the 2p, 2s states of O, and 3d states of Zn. Meanwhile, multiple characteristic peaks can be seen in the valence band XPS of pure ZnO, in which the strong peak at 10.4 eV is mainly contributed by the hybridization of O 2p and Zn 3d4s, the peak at 3.1 eV–5 eV is mainly from O 2p.[36] Figure 6(b) shows the valance band XPS of Ag, in which the peak position of 4.5 eV is contributed by the Ag 4d.[37,38] Figure 6(c) is the valance band XPS of the ZnO substrate with the grown Ag film without any treatment (ZnO/Ag). As expected, it is only a simple superposition of the valance band XPS spectra of those from Ag and ZnO. This proves that the valence band structure of the Ag and ZnO mixture is just a simple superposition when they are mixed without interaction.

Figure 6(d) is the valence band XPS of ZnO:Ag. As can be seen, the intensity at 3 eV–6 eV, which is related to the characteristics of Ag, decreases gradually from the depth of 100 nm to 400 nm, showing that the concentration of Ag decreases with the increasing of the depth, in good agreement with the previous results from EDS and XPS. Although the binding energy of Zn 2p maintains at the position of 10 eV at the depth of 100 nm–400 nm, there appears a shift of −0.4 eV relative to the surface. This demonstrates that the doping of Ag has an impact on the Zn 2p states, which is consistent with the calculations based on density functional theory.[38] The inset of Fig. 6(d) in the upper right shows the enlarged view of the binding energy range from −1 eV to 4 eV. It can be found from the enlarged view of the band edge that the leading edge of the valence-band spectra of the Ag-doped ZnO moves to 0 eV with increasing depth. The presence of Ag^{+} ions in the ZnO lattice creates additional energy levels near the valence band of ZnO. This change also contributes to the increase in bandgap along with increased states in the conduction band.[39]

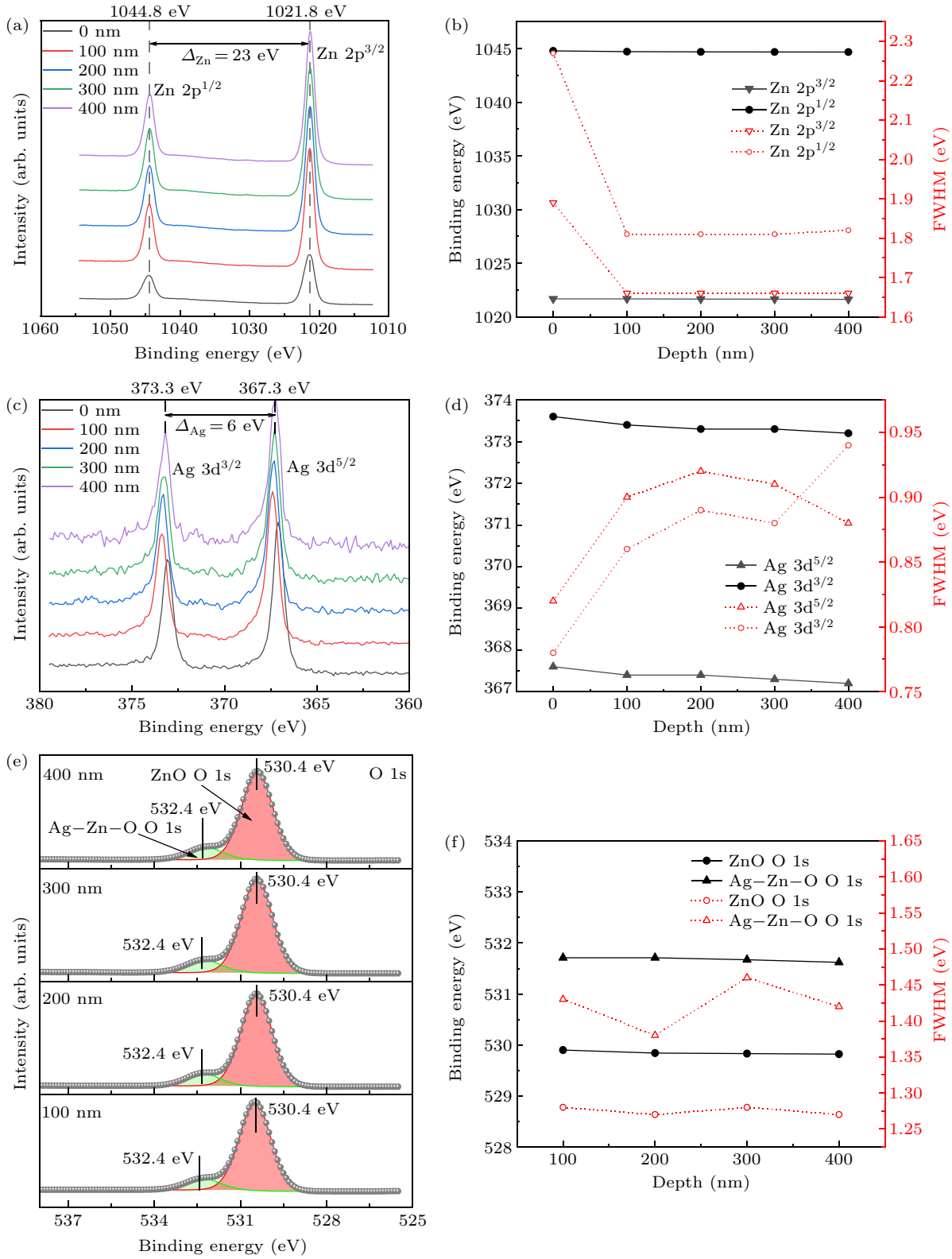


Fig. 5. XPS analysis of ZnO:Ag. Core level XPS for (a) Zn 2p, (c) Ag 3d, and (e) O 1s. The peak position (solid line with symbol, left-hand side) and FWHM (dotted line with symbol, right-hand side) of ZnO:Ag as a function of depth (in unit nm) for (b) Ag 3d, (d) Zn 2p, and (f) O 1s.

To determine whether ZnO:Ag is a simple mixture of ZnO and Ag, the valence band XPS of pure Ag and pure ZnO are theoretically mixed according to the atomic concentration ratio of Ag and Zn determined by XPS (see Table 2) at distinctive depths, and then compared with the experimental (ZnO:Ag) valence band XPS. All used XPS intensities have been normalized. The misfit between the theoretical mixing and the experimental data is determined by using their difference spectra:[40]

$$\Delta I_n = I_{\text{exp}} - I_{\text{mix}},$$

where I_{exp} is the intensity of valence band XPS of ZnO:Ag.

I_{mix} is the theoretically mixing intensity of valence band XPS and n is the depth ($n = 0$ nm, 100 nm, 200 nm, 300 nm, 400 nm). The formula of I_{mix} is: $I_{mix} = aI_{Ag} + bI_{ZnO}$, which assumes that the XPS spectrum of the Ag-dope ZnO sample would be a superposition of the emission from the pure Ag I_{Ag} and pure ZnO I_{ZnO}, with each weighted by normalization coefficients a and b according to their atomic concentration ratios (Table 2). The existence of other component and electronic state evolution of the ZnO:Ag, other than pure Ag and pure ZnO, can then be inferred by the level of misfit of the theoretical mixture valence band XPS compared with the experimental valence band XPS. The fitting results from Fig. 7 can be explicitly contented that the theoretical mixing of valence bands of ZnO and Ag at different depths is not appropriate to match the valence band XPS of ZnO:Ag. There exist distinct levels of the misfit in different binding energy, which means that Zn and Ag elements have diverse forms of orbital overlap at different depths, resulting in different mixtures of Zn, O, and Ag. Figure 7 show the difference spectra of around −1.8 eV to 20 eV, and it can be seen that there is obviously positive misfit around 4 eV, which indicates that additional electronic states of Ag 4d and O 2p appear compared with the non-interacting mixed state, and then infers that the silver element does not only exist in the form of metallic silver but could appear as Ag_2O or an alloy (ZnAgO), in agreement with the XRD result. Likewise, there is a positive misfit at 7 eV, which is associated with Zn 3d4s and O 2p states, thus it can be further confirmed that there is an alloy composed of Zn, O, and Ag. The manifestly positive misfit can be found near 9.8 eV, which is due to the displacement between ZnO: Ag and pure ZnO. However, the negative misfit at 11 eV is attributed to the characteristic Zn 3p hybridization peak of ZnO. This means that Zn 3p is reduced because of Ag incorporation.

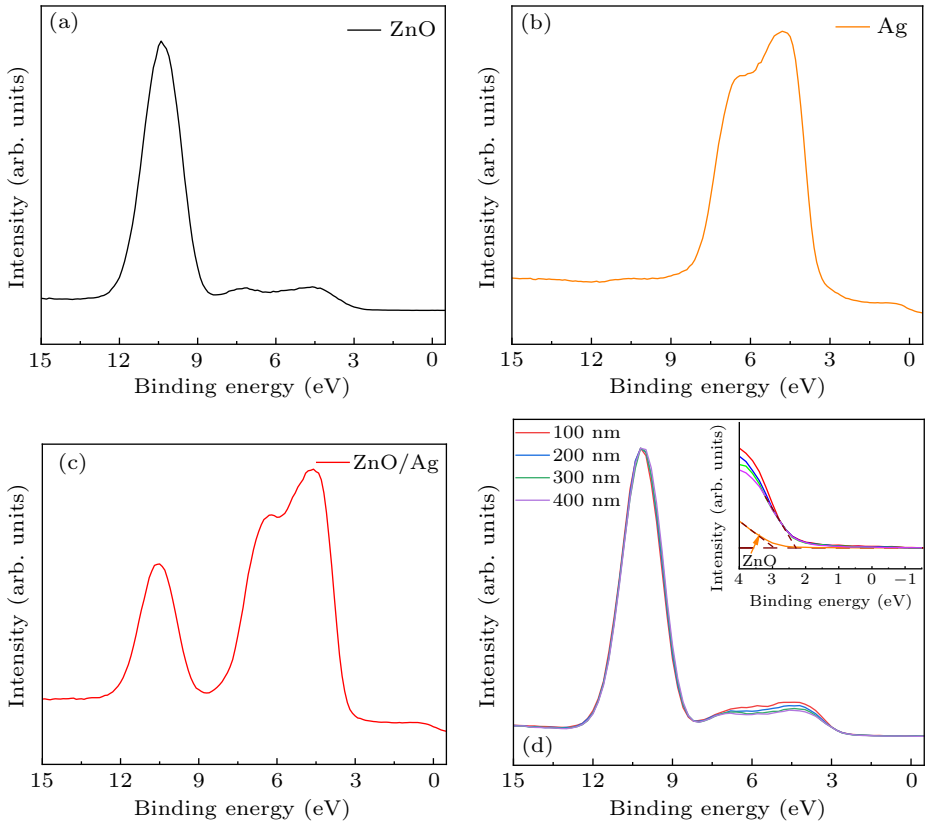


Fig. 6. Valance band XPS of (a) pure ZnO, (b) pure Ag, (c) ZnO with capped Ag before laser treatment, ZnO/Ag, (d) laser-induced doped Ag in ZnO, namely, ZnO:Ag.

As mentioned earlier, doping is one of the effective ways to improve the thermoelectric properties of materials.[26–29] In principle, the increase of electric conductivity and the decrease of thermal conductivity are beneficial to the thermoelectric performance.[41] From the inset of Fig. 6(d), it is possible that the electric conductivity of the Ag-doped ZnO with a narrower bandgap would be higher than the pure ZnO. The comparison of the thermal diffusivity of ZnO and ZnO:Ag is given in Fig. 8, in which a decrease in the thermal diffusivity can be found after doping. This proves that doping has a positive effect on the reduction of thermal diffusivity. The reason for the decrease in thermal diffusivity is that phonons are subject to different scattering mechanisms during transport. The more they are scattered, the shorter mean free path they would have and the lower their thermal diffusivity. The doping results in more impurity scattering and defect scatter-

ing in the lattice, which hinders the transport of phonons and reduces the thermal diffusivity.[42–44] The reduction of thermal diffusivity is obvious in the low-temperature range around room temperature to 400 K and beyond 1000 K. This makes ZnO:Ag prospect thermoelectric applications at low and high temperatures.

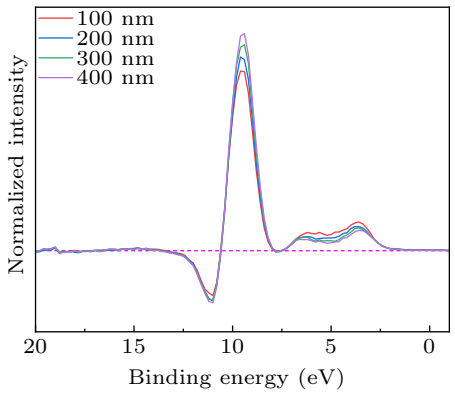


Fig. 7. The difference spectra ΔI_n between the experimental spectra and the model spectra by theoretical mixing.

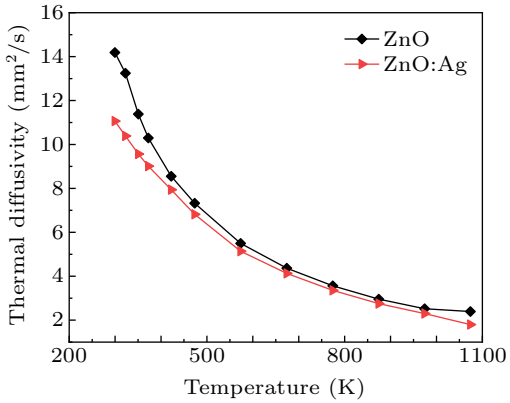


Fig. 8. The thermal diffusivity of ZnO and ZnO:Ag as a function of temperature.

3.3. Prospective of laser-induced doping method

One of the key features of laser-induced doping is that the doping distribution is depth-dependent. For example, in our samples, the interesting point is that the Ag distribution in ZnO exhibits the gradient feature from the surface to the bulk. Such characteristics make ZnO:Ag a promising graded material for special applications. As shown in our previous work,[45] microstructured cellular biomorphic materials, such as bamboo or coconut-shell charcoals, exhibit gradient microstructures, which can be used to design highly efficient thermal rectifiers. Graded material ZnO:Ag, as presented in this work, may have gradient-dependent properties, including the gradient-dependent thermal conductivity. It is speculated that ZnO:Ag may have interesting thermal rectification. This can be justified by two features: (i) as aforementioned in the previous section, the XPS and SIMS results clearly demonstrated the gradient feature of ZnO:Ag, which would lead to gradient-dependent thermal conductivity; and (ii) the averaged thermal diffusion of ZnO:Ag showed the obvious difference from that of the pure ZnO, especially near the room temperature. These two features can be utilized to design multi-segment thermal rectifiers, as demonstrated in our recent simulations.[46]

By applying pressure[47] including strain engineering[48–52] or applying "chemical pressure" with chemical impurities[53] or alloying,[54] it is possible to tune properties of functional materials in different ways. Laser-induced method provides an alternative approach for doping with the advantage of flexibility by post-treatment and enables selected-area doping.

It is also possible to extend the application of laser-induced technique for other material doping, for example, fabrication of diluted magnetic semiconductors through the doping of magnetic elements. Half-metal[48] or doping magnetic elements in semiconductor[55–57] are important candidates for applications in spintronics. The doping magnetic elements with laser-induced technique may have some advantage or unique features. For example, the cluster-like doping rather than point doping could have larger magnetic domains, and the gradient element distribution may provide additional channels for tuning magnetic interactions.

The unique structural and electronic properties of depth-dependent doping system can be further characterized using a combination of advanced techniques,[40,58–61] such as the integrated study of synchrotron radiation, electron microscopy, and first-principles calculations.[58–61]

4. Conclusion

In summary, we presented an innovative laser-induced method for the synthesis of Ag-doped ZnO. This method provides an effective doping strategy. The analysis of XRD and SEM shows that the samples maintain the single crystal structure after laser irradiation. The results of core level XPS and TOF-SIMS show that the ZnO distribution in the samples remains uniform, but the Ag concentration decreases with increasing depth. The analysis of electronic state evolution is supplied by core level and valence band XPS, which demonstrates that silver dopants could exist in the form of metallic silver, silver oxide and Zn–Ag–O alloys. The electronic and thermal properties of the Ag-doped ZnO indicate its promising thermoelectric applications.

Acknowledgment

Project supported by the National Key Research and Development Program of China (Grant No. 2022YFB3605403).

References

[1] Look D C 2001 *Mater. Sci. Eng. B* **80** 383
[2] Wang Z L 2004 *J. Phys.: Condens. Mater.* **16** R829
[3] Hu J Q, Bando Y, Zhan J H, Li Y B and Sekiguchi T 2003 *Appl. Phys. Lett.* **83** 4414

[4] Shen X, Allen P B, Muckerman J T, Davenport J W and Zheng J C 2007 *Nano Lett.* **7** 2267
[5] Liu J, Xu Y and Yi F 2022 *Sensor. Actuat. A-Phys.* **345** 113665
[6] Fulati A, Ali S M U, Riaz M, Amin G, Nur O and Willander M 2009 *Sensors* **9** 8911
[7] Kim S W, Ueda M, Kotani T, Fujita S and Fujita S 2003 *Appl. Phys. Lett* **83** 3593
[8] Li W, Wu X, Han N, Chen J, Qian X, Deng Y, Tang W and Chen Y 2016 *Sensors Actuat. B-Chem.* **225** 158
[9] Ding Y, Kong X Y and Wang Z L 2004 *Phys. Rev. B* **70** 235408
[10] Zhou H, Wu L, Wang H Q, Zheng J C, Zhang L, Kisslinger K, Li Y, Wang Z, Cheng H, Ke S, Li Y, Kang J and Zhu Y 2017 *Nat. Commun.* **8** 1474
[11] Zhou H, Wang H Q, Zheng J C, Wang X D, Zhang Y, Kang J, Zhang L, Kisslinger K, Wu R, Wang J O, Qian H J and Ibrahim K 2021 *Appl. Surf. Sci.* **570** 151189
[12] Liang X, Zhou H, Wang H Q, Zhang L, Kisslinger K and Kang J 2021 *Chin. Phys. B* **30** 096107
[13] Qi K, Xing X H, Jung D Y, Zada A, Li M Y, Wang Q, Liu S Y, Lin H X and Wang G Z 2020 *Ceram. Int.* **46** 1494
[14] Selim F A, Tarun M C, Wall D E, Boatner L A and McCluskey M D 2012 *Appl. Phys. Lett.* **99** 202109
[15] Ma Z H, Ren F Z, Ming X L, Long Y Q and Volinsky A A 2019 *Materials* **12** 196
[16] Tang K, Gu S L, Ye J D, Zhu S M, Zhang R and Zheng Y D 2017 *Chin. Phys. B* **26** 047702
[17] De Lourdes Ruiz Peralta M, Pal U, and Sanchez Zeferino R 2012 *ACS Appl. Mater. Interfaces* **4** 4807
[18] Ma L, Zhang Q, Li J, Lu X, Gao C, Song P and Xia L 2021 *Materials* **14** 992
[19] Ahn D B, Kang H S, Kim J H, Kim G H, Chang H W and Lee S Y 2006 *J. Appl. Phys.* **100** 093701
[20] Swapna R and Santhosh Kumar M C 2013 *Ceram. Int.* **39** 1799
[21] Chen R, Fan B, Pan M, Cheng Q and Chen C 2016 *Mater. Lett.* **163** 90
[22] Aoki T, Hatanaka Y and Look D C 2000 *Appl. Phys. Lett.* **76** 3257
[23] Choi I, Jeong H Y, Jung D Y, Byunc M, Choi C G, Hong B H and Choi S Y and Lee K J 2014 *ACS Nano* **8** 7671
[24] Tian Z, Slama I A, Quick N R and Kar A 2005 *Acta Mater.* **53** 2835
[25] Chizhik A B, Davidenko I I, Maziewski A and Stupakiewicz A 1998 *Phys. Rev. B* **57** 14366
[26] He J, Zhao L D, Zheng J C, Doak J W, Wu H, Wang H Q, Lee Y, Wolverton C, Kanatzidis M G and Dravid V P 2013 *J. Am. Chem. Soc.* **135** 4624
[27] He J, Blum I D, Wang H Q, Girard S N, Doak J, Zhao L D, Zheng J C, Casillas G, Wolverton C, Jose-Yacaman M, Seidman D N, Kanatzidis M G and Dravid V P 2012 *Nano Lett.* **12** 5979
[28] He J, Sootsman J R, Girard S N, Zheng J C, Wen J, Zhu Y, Kanatzidis M G and Dravid V P 2010 *J. Am. Chem. Soc.* **132** 8669
[29] He J, Sootsman J R, Xu L Q, Girard S N, Zheng J C, Kanatzidis M G and Dravid V P 2011 *J. Am. Chem. Soc.* **133** 8786
[30] Zheng J C 2022 *Research* **2022** 9867639
[31] Li J, Li Y, Li S, Zhu M, Zhang J, Li Y, He Y and Li W 2020 *Ceram. Inter.* **46** 18639
[32] Habibi M H and Sheibani R 2010 *J. Sol-Gel Sci. Techn.* **54** 195
[33] Yıldırım Ö A, Unalan H E, Durucan C and Klein L 2013 *J. Am. Chem. Soc.* **96** 766
[34] Gerrard N L, Coultas S J and Counsell J D P 2022 *Surf. Sci. Spectra* **29** 014009
[35] Tao J, Lu H L, Gu Y, Ma H P, Li X, Chen J X, Liu W J, Zhang H and Feng J J 2019 *Appl. Surf. Sci.* **476** 733
[36] Li Y, Wang H Q, Ibrahim K, Wang J O, Wu R, Qian H J, Wang H, Lei T, Wang Z, Li X, Wu M, Zheng J C, Kang J, Zhang L, Kisslinger K, Wu L and Zhu Y 2020 *Phys. Rev. Mater.* **4** 124601
[37] Xie F W, Yang P, Li P and Zhang L Q 2012 *Opt. Commun.* **285** 2660
[38] Zhang X D, Guo M L, Shen Y Y, Liu C L, Xue Y H, Zhu F and Zhang L H 2012 *Comp. Mater. Sci.* **54** 75
[39] Poduval G K, Duan L, Hossain M A, Sang B, Zhang Y, Zou Y, Uddin A and Hoex B 2020 *Solar RRL* **4** 2000241
[40] Wang H Q, Xu J Y, Lin X Y, Li Y P, Kang J Y and Zheng J C 2021 *Light Sci. Appl.* **10** 153
[41] Zheng J C 2008 *Front. Phys. China* **3** 269
[42] Ohtaki M, Tsubota T, Eguchi K and Arai H 1996 *J. Appl. Phys.* **79** 1816
[43] Snyder G J and Toberer E S 2008 *Nat. Matter.* **7** 105
[44] Delorme F, Diaz-Chao P, Guilmeau E and Giovannelli F 2015 *Cerma. Int.* **41** 10038
[45] Li X J, Li N, Ren F, Wang K H, Koh C L, Wu M, Wang H Q and Zheng J C 2018 *J. Mater. Sci.* **53** 13955
[46] Du F Y, Zhang W, Wang H Q and Zheng J C 2023 *Chin. Phys. B* **32** 064402
[47] Wang X D, Zhou H, Wang H Q, Ren F, Chen X H, Zhan H H, Zhou Y H and Kang J Y 2015 *Chin. Phys. B* **24** 097106
[48] Zheng J C and Davenport J W 2004 *Phys. Rev. B* **69** 144415
[49] Zhu Y and Zheng J C 2006 *Phys. Rev. B* **73** 024509
[50] Huang Z, Lü T Y, Wang H Q, Yang S W and Zheng J C 2017 *Comput. Mater. Sci.* **130** 232
[51] Cheng H and Zheng J C 2021 *Front. Phys.* **16** 43505
[52] Li J J, Dai Y and Zheng J C 2022 *Front. Phys.* **17** 13503
[53] Li D H, Wang H Q, Zhou H, Li Y P, Huang Z, Zheng J C, Wang J O, Qian H J, Ibrahim K, Chen X, Zhan H, Zhou Y and Kang J 2016 *Chin. Phys. B* **25** 076105
[54] Liang X, Zhou H, Wang H Q, Zhang L, Kisslinger K and Kang J 2021 *Chin. Phys. B* **30** 096107
[55] Liao X X, Wang H Q and Zheng J C 2013 *J. Am. Ceram. Soc.* **96** 538
[56] Zeng H, Wu M, Wang H Q, Zheng J C and Kang J 2020 *Materials* **13** 5686
[57] Zeng H, Wu M, Wang H Q, Zheng J C and Kang J 2021 *Front. Phys.* **16** 43501
[58] Zheng J C, Wu L, Zhu Y and Davenport J W 2005 *J. Appl. Crystallogr.* **38** 648
[59] Zheng J C, Wu L and Zhu Y 2009 *J. Appl. Crystallogr.* **42** 1043
[60] Zheng J C, Frenkel A I, Wu L, Hanson J, Ku W, Božin E S, Billinge S J L and Zhu Y 2010 *Phys. Rev. B* **81** 144203
[61] Zheng J C and Wang H Q 2021 *Sci. China Phys. Mech.* **51** 030007